Eur. Phys. J. B (2016) 89: 177
DOI: 10.1140/epjb/e2016-60988-6

THE EUROPEAN PHYSICAL JOURNAL B

Regular Article

The effects of cup-like and hill-like parabolic confining potentials on photoionization cross section of a donor in a spherical quantum dot

Moletlanyi Tshipa[a]

University of Botswana, Private Bag 0022, Gaborone, Botswana

Received 31 December 2015 / Received in final form 30 April 2016
Published online 8 August 2016 –

Abstract. A theoretical investigation of the effects of hill-like and cup-like parabolic confining electric potentials on photoionization cross section (PCS) in a spherical quantum dot is presented. The hill-like and the cup-like parabolic potentials are superimposed on an infinite spherical square well (ISSW) potential. As the cup-like parabolic potential intensifies, the peak of the PCS becomes redshifted for the $s \rightarrow p$ transition, and becomes blueshifted for the $p \rightarrow d$, $d \rightarrow f$ (and so forth) transitions. The hill-like parabolic potential, on the contrary, blueshifts peaks of the PCS for $s \rightarrow p$ transitions, while it redshifts those of transitions between higher states as it intensifies. Consequently, the two potentials discriminate between transitions involving the ground state and those involving higher states.

1 Introduction

Realization of nanostructures of different dimensions and geometries has been beneficial to the scientific community and the world at large, because of applications and possible applications in a wide range of disciplines like biomedicine and other social remedies [1], gas sensing [2], optoelectronics [3,4] and thermoelectric applications [5,6], among others. The mushrooming of different techniques of obtaining a plethora of nanostructures has prompted both theoretical and experimental research into these structures. Among quantum phenomena probed, photoionization is equally appealing. The effect of anisotropy of quantum confinement on photoionization cross section (PCS) has been probed, and was shown to be appreciable for certain degree of anisotropies [7]. Influences of electric fields and intense laser fields on PCS have been also reported on, revealing a blueshift of the peak of the PCS with increasing laser strength [8]. PCS of a trion (a hole or an electron bound to an exciton) was probed by Xie, and how it is affected by pressure, parabolic confinement frequency and hole mass [9]. Apart from parabolic confinement, the other confining potential topography which has been studied is the power-exponential [10]. PCS of quantum rings has also been reported, and how it is influenced by the size of the inner radius of the rings [11] and by externally applied magnetic field [12,13]. The role that impurity position plays in modifying the PCS in a core-shell nanodot has been investigated [14]. In this communication, the effects of cup-like and hill-like parabolic confining potentials on PCS of a donor in a spherical quantum dot (SQD) are investigated.

[a] e-mail: tshipam@mopipi.ub.bw

2 Theoretical model

2.1 Photoionization cross section

The system investigated is a spherical quantum dot (SQD), which may be a GaAs material embedded in a $Ga_{1-x}Al_xAs$ matrix, with a donor impurity entrenched at the centre. The potentials inside the spherical dot assume parabolic geometries. A bi-parabolic (cup-like) potential is contrasted with an inverse lateral bi-parabolic (hill-like) potential, each superimposed on an infinite spherical square well (ISSW). Photoionization cross section, which can be regarded as the probability that a bound electron can be liberated by some appropriate radiation per unit time per unit area, is given by [8–12]

$$\sigma_{lm} = \sigma_0 \hbar\omega \sum_f |\langle f|\boldsymbol{r}|i\rangle|^2 \delta(E_f - E_i - \hbar\omega) \qquad (1)$$

with

$$\delta(E_f - E_i - \hbar\omega) = \frac{\hbar\Gamma}{(E_f - E_i - \hbar\omega)^2 + (\hbar\Gamma)^2}, \qquad (2)$$

where $\hbar\omega$ is photon energy, Γ the impurity linewidth and $\sigma_0 = \frac{4\pi^2 \alpha_{FS} n}{3\epsilon_m}(\frac{E_{in}}{E_{av}})^2$. E_{in} is the effective incident electric field while E_{av} is the average electric field in the dot of refractive index n and dielectric constant ϵ_m. E_i and E_f are energies associated with initial and final eigenstates $|i\rangle$ and $|f\rangle$, respectively. $\langle f|\boldsymbol{r}|i\rangle$ is the usual interaction integral coupling initial states to final states, α_{FS} is the fine structure constant and $\boldsymbol{r}$ is electron position vector. The wave functions are obtainable as solutions to the Schrödinger equation with the form

$\Psi_{lm}(\rho,\theta,\phi) = C_{lm}Y_{lm}(\theta,\phi)\chi(\rho)$, dependent on the potential, where $\chi(\rho)$ is the radial component of the wave function satisfying the Schrödinger equation

$$\frac{1}{\rho^2}\frac{d}{d\rho}\left(\rho^2\frac{d}{d\rho}\chi(\rho)\right)+\left\{\frac{2\mu}{\hbar^2}[E_{lm}+\frac{k_e e^2}{\epsilon_m\rho}-V(\rho)]-\frac{l(l+1)}{\rho^2}\right\}\times\chi(\rho)=0 \quad (3)$$

with μ being effective mass of electron (of charge $-e$) and k_e the Coulomb constant. The orbital momentum quantum number, $l(l=0,1,2,\ldots)$, quantifies angular momenta of electrons in different states. $Y_{lm}(\theta,\phi)$ are the usual spherical harmonics, m being the magnetic quantum number and C_{lm} the normalization constant. Evaluation of the interaction integral leads to the selections rules $\Delta l = \pm 1$, between the initial and final states [10].

2.2 The wave functions

2.2.1 The bi-parabolic (cup-like) potential

The bi-parabolic potential superimposed on an ISSW has the mathematical form

$$V(\rho) = \frac{1}{2}\mu\omega_0^2(\rho - R/2)^2 \quad (\rho < R)$$

and infinity elsewhere. If, after insertion of the expression for the bi-parabolic potential into the Schrödinger equation, one makes the transformation

$$\chi(\rho) = \rho^l e^{\frac{\mu\omega_0}{2\hbar}(\rho-R)\rho}F(\rho),$$

then, in the presence of the impurity, $F(\rho)$ satisfies the second order differential equation

$$\frac{d^2F(\rho)}{d\rho^2}-\frac{dF(\rho)}{\rho d\rho}\left[\frac{\mu\omega_0}{\hbar}(R-2\rho)\rho-2(l+1)\right]-\frac{F(\rho)}{\rho}\left\{\frac{\mu\omega_0}{\hbar}[R(l+1)-(2l+3)\rho]+\frac{2\mu\rho}{\hbar^2}\left(E+\frac{k_e e^2}{\epsilon}\right)\right\}=0. \quad (4)$$

If we let

$$z = -i\sqrt{\frac{\mu\omega_0}{\hbar}}\rho$$

then equation (4) can then be recast as:

$$\frac{d^2F(z)}{dz^2}-\frac{dF(z)}{zdz}\left[2z^2+iR\sqrt{\frac{\mu\omega_0}{\hbar}}z-2(l+1)\right]-\frac{F(z)}{2z}\left\{\left[2(2l+3)+\frac{4E}{\hbar\omega_0}\right]z+2i\sqrt{\frac{\mu\omega_0}{\hbar}}(l+1)R+\frac{4ik_e e^2}{\epsilon\hbar}\sqrt{\frac{\mu}{\hbar\omega_0}}\right\}=0, \quad (5)$$

which is a Heun biconfluent equation whose solution is [15,16];

$$F(z) = HeunB(|2l+1|,\alpha,\beta,\gamma,z) \quad (6)$$

with

$$\alpha = iR\sqrt{\frac{\mu\omega_0}{\hbar}}$$
$$\beta = -\frac{2E_{lm}}{\hbar\omega_0}$$
$$\gamma = -\frac{4ik_e e^2}{\hbar\epsilon_m}\sqrt{\frac{\mu}{\hbar\omega_0}}, \quad (7)$$

therefore the solution can be written as:

$$\chi(\rho) = e^{g_1(\rho)}\rho^l HeunB(2l+1,\alpha,\beta,\gamma,g_2(\rho)) \quad (8)$$

with the arguments

$$g_1(\rho) = \frac{\mu\omega_0}{2\hbar}(\rho - R)\rho \quad (9)$$

and

$$g_2(\rho) = -i\sqrt{\frac{\mu\omega_0}{\hbar}}\rho. \quad (10)$$

Requiring that the electron wave function should vanish at the walls of the SQD, the energy spectrum for an electron in an SQD with an intrinsic bi-parabolic potential is availed as:

$$E_{lm} = -\frac{1}{2}\beta_E\hbar\omega_0 \quad (11)$$

where β_E is the value of β that satisfies the condition

$$HeunB(2l+1,\alpha,\beta_E,\gamma,g_1(R)) = 0. \quad (12)$$

Disregarding the electron-impurity interaction, the Schrödinger equation is still solvable in terms of the Heun biconfluent function (Eq. (8)) with parameters being identical to those for this potential in the presence of the donor impurity equations (7), (9), (10) except for $\gamma = 0$ and $\beta^0 = -\frac{2E^0_{lm}}{\hbar\omega_0}$, availing the energies without the Coulombic interaction as:

$$E^0_{lm} = -\frac{1}{2}\beta^0_E\hbar\omega_0, \quad (13)$$

where β^0_E is the value of $\beta = \beta^0$ that satisfies the condition specified in equation (12).

2.2.2 The inverse lateral bi-parabolic (hill-like) potential

This potential is minimum at the centre of the SQD, and concavely increases parabolically to attain a maximum at a radial distance half the radius of the SQD. It then concavely decreases to its minimum at the walls of the SQD $(\rho = R)$;

$$V(\rho) = \frac{1}{2}\mu\omega_0^2(R\rho - \rho^2) \quad (\rho < R)$$

and infinity elsewhere. Inserting this expression for the inverse lateral shifted parabolic potential into the Schrödinger equation in the presence of the impurity and letting

$$\chi(\rho) = \rho^l e^{\frac{\mu\omega_0}{2i\hbar}(R-\rho)\rho}F(\rho)$$

leaves the radial component of the Schrödinger equation reading as:

$$\frac{d^2F(\rho)}{d\rho^2} - \frac{dF(\rho)}{\rho d\rho}\left[\frac{i\mu\omega_0}{\hbar}(R-2\rho)\rho - 2(l+1)\right] - \frac{F(\rho)}{\rho}\left\{\left[\frac{i\mu\omega_0}{\hbar}(2l+3) + \frac{\mu^2\omega_0^2R^2}{4\hbar^2} - \frac{2\mu E}{\hbar^2}\right]\rho - \frac{i\mu\omega_0}{\hbar}(l+1)R - \frac{2\mu k_e e^2}{\epsilon\hbar^2}\right\} = 0. \quad (14)$$

A further substitution

$$z = \sqrt{\frac{-i\mu\omega_0}{\hbar}}\rho$$

morphs equation (14) into

$$\frac{d^2F(z)}{dz^2} - \frac{dF(z)}{zdz}\left[2z^2 + iR\sqrt{\frac{\mu\omega_0}{-i\hbar}}z - 2(l+1)\right] - \frac{F(z)}{2z}\left\{\left[2(2l+3) - \frac{\mu\omega_0R^2}{2i\hbar} + \frac{4E}{i\hbar\omega_0}\right]z + 2\sqrt{\frac{-i\mu\omega_0}{\hbar}}(l+1)R + \frac{4k_e e^2}{\epsilon i\hbar}\sqrt{\frac{-i\mu}{\hbar\omega_0}}\right\} = 0, \quad (15)$$

which is also solvable in terms of the Heun biconfluent function (Eq. (6)) but with

$$\alpha = R\sqrt{\frac{\mu\omega_0}{i\hbar}}$$
$$\beta = \frac{\mu\omega_0^2R^2 - 8E_{lm}}{4i\hbar\omega_0}$$
$$\gamma = \frac{4k_e e^2}{\hbar\epsilon_m}\sqrt{\frac{-\mu}{i\hbar\omega_0}}. \quad (16)$$

Thus, the radial component of the wave function for a hill-like parabolic potential in a spherical quantum dot is given by equation (8) with

$$g_1(\rho) = \frac{\mu\omega_0}{2i\hbar}(R-\rho)\rho \quad (17)$$

and

$$g_2(\rho) = \sqrt{\frac{-i\mu\omega_0}{\hbar}}\rho. \quad (18)$$

Application of the boundary conditions at the walls of the SQD avails the energy spectrum as:

$$E_{lm} = \frac{1}{8}\mu\omega_0^2R^2 - \frac{i\beta_E}{2}\hbar\omega_0, \quad (19)$$

with β_E being the value of β that satisfies the condition set in equation (12).

In the absence of the impurity, the parameters have the same expressions as those for this potential in the presence of the impurity (Eqs. (16)–(18)) with the exception of $\gamma = 0$ and $\beta^0 = \frac{\mu\omega_0^2R^2 - 8E^0_{lm}}{4i\hbar\omega_0}$, hence the energy

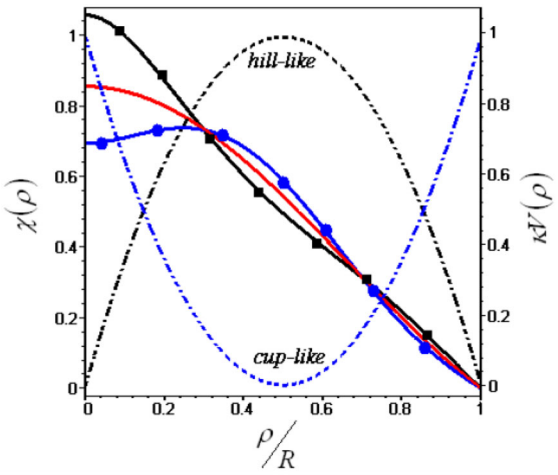

Fig. 1. The effects of the two parabolic potentials (which are the dash-dotted curves) on the ground state radial electron wave functions across an SQD. The plot marked with dots corresponds to the ground state wave function in an SQD with a cup-like parabolic potential while the one marked with squares is associated with the hill-like parabolic potential, each of strength ($\hbar\omega_0 = 15$ meV). The solid unmarked plot is the ground state radial wave function in an SQD with a purely ISSW ($\hbar\omega_0 = 0$ meV).

associated with the hill-like parabolic potential without the Coulombic interaction can be cast in the form

$$E^0_{lm} = \frac{1}{8}\mu\omega_0^2R^2 - \frac{i\beta^0_E}{2}\hbar\omega_0, \quad (20)$$

β^0_E still being the value of $\beta = \beta^0$ that satisfies the condition stipulated in equation (12).

3 Results

This section is dedicated to discussions and analysis of the results. The parameters used in the computations are $\mu = 0.067m_e$, m_e being the free electron mass and $\epsilon_m = 12.5$, pertaining to GaAs nanodots. Although the discussions here include transitions between higher states, for succinctness, the PCS illustrated in the this paper are associated with the $s \rightarrow p$ transitions only. The geometries of the confining potentials are illustrated in Figure 1, which depicts the influence of these potentials on the radial component of the ground state electron wave function, with $\kappa = [2/(\mu\omega_0^2R^2)]$. By virtue of the fact that the cup-like parabolic potential is maximum at the centre and at the walls of the SQD, the ground state electron wave function at those regions is reduced, and the reduction increases with increasing potential intensity. For excited states, the electron wave functions are merely tightened around a radial distance half the radius of the SQD.The hill-like potential, contrastingly, is most intense at the radial distance half the radius of the SQD ($r_0 = \rho = 0.5R$), and thus dwindles electron wave functions at this radial distance, enhancing them elsewhere, as it gets stronger.

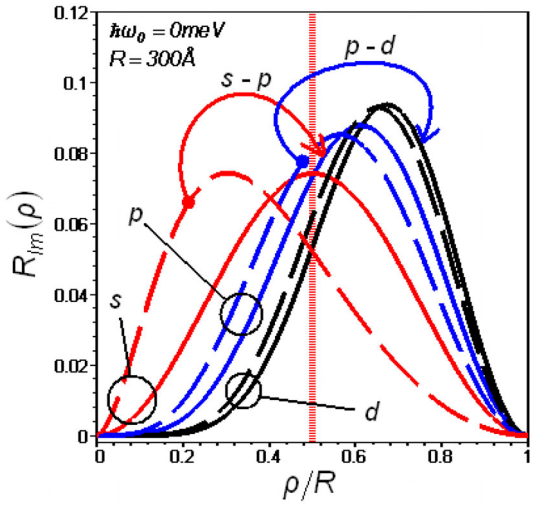

Fig. 2. The radial probability densities of the first three lowest lying states. The solid plots represent radial probability densities in the absence of the impurity while the dashed are associated with the presence of the donor impurity.

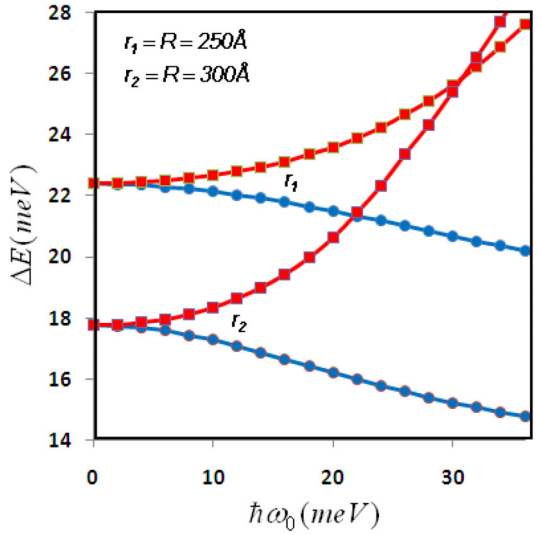

Fig. 3. The energy differences between the ground state (s) and the first excited state (p) as functions of strengths of the parabolic potentials for the indicated radii of the SQD; the plots marked with dots are associated with the cup-like parabolic potential while those marked with squares are associated with the hill-like parabolic potential.

The presence of either the hill-like parabolic potential or the cup like parabolic potential will, of course, shift peaks of the probability densities, but this will have no bearing on the reasoning that follows. The most probable radial position of the ground state is in a region where the hill-like (cup-like) parabolic potential is less (more) intense than at the radial expectation value of the first excited state. The hill-like parabolic potential shifts peaks of probability densities of the ground towards the centre, and those of the excited states towards the walls of the SQD, expelling electrons away from a region where it (the hill-like parabolic potential) is maximum (at $r_0 = \rho = 0.5R$). Contrastingly, the cup-like parabolic potential shifts peaks of probability densities towards r_0, where the potential is minimum. Consequently, the hill-like (cup-like) parabolic potential perturbs the first excited state (ground state) more than it does the ground state (excited states), thus the potential has the propensity to increase (reduce) $s \rightarrow p$ transition energies ($\Delta E = E_f - E_i$) as it intensifies. Contrastively, the second excited state electron spends most of its time where the hill-like (cup-like) parabolic potential is weaker (stronger) than at the radial position expectation value of the first excited state. This can be seen in Figure 2 where the variations of radial probability densities ($R_{lm}(\rho) = \rho^2\chi(\rho)^2$) of the first three lowest lying states have been graphically illustrated. The vertical line represents r_0, where the hill-like (cup-like) parabolic potential is maximum (minimum). The arrows represent the allowed photoionization transitions from the two lowest lying states in the dipole regime. As such, the hill-like (cup-like) parabolic potential naturally diminishes (enhances) transition energies associated with the first and second excited states, as well as between higher states (Fig. 3). Effectively, the hill-like (cup-like) parabolic potential redshifts (blueshifts) peaks of $p \rightarrow d$ PCS and those of higher states, while it blueshifts (redshifts) peaks of $s \rightarrow p$ PCS, as it intensifies.

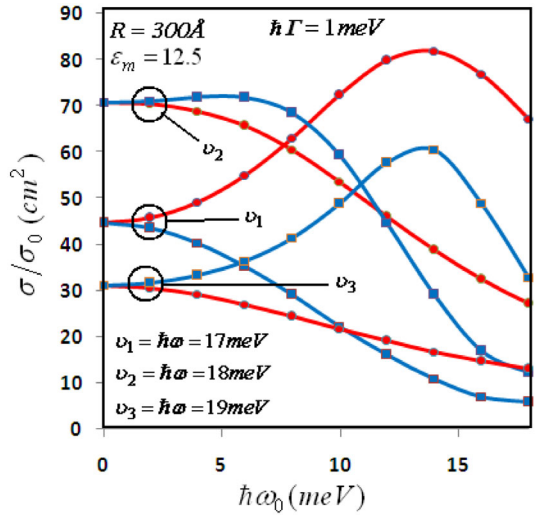

Fig. 4. The variation of the normalized PCS with strengths of the cup-like (curves with dots) and the hill-like (marked with squares) parabolic potentials for the different beam energies of excitation.

The energy difference between the s and p states in an SQD of radius 300 Å is in the vicinity of 17.762 meV in the absence of the parabolic potentials ($\hbar\omega_0 = 0$ meV). Figure 4 shows the dependence of the normalized PCS for a spherical quantum dot of such dimensions on strengths of the parabolic potentials. Thus, if the beam energy of excitation is less than $\hbar\omega_0 = 0$ transition energies, then the cup-like parabolic potential can be utilized to capacitate $s \rightarrow p$ photoionization (and demote photoionization from higher states) while the hill-like parabolic potential facilitates photoionization from higher states (demoting $s \rightarrow p$ photoionization).

Because transition energy scales inversely with the radius of the SQD, the two potentials afford us the ability to modulate transition energies without necessarily having to tamper with the dimensions of SQDs. This is advantageous in cases where excitation energy is to have a specific value which an ISSW quantum dot of the required radius may not have.

4 Conclusions

Analytical expressions for electron wave functions in a spherical quantum dot with and without a centred donor impurity have been obtained and utilized to probe the effects of the cup-like and hill-like parabolic potentials on PCS in an SQD. The two parabolic potentials exhibit selective enhancement and reduction of transition energies: hill-like (cup-like) parabolic potential enhancing (dwindling) transition energies involving the ground state and dwindling (enhancing) those involving higher states. Consequently, the hill-like (cup-like) parabolic potential blueshifts (redshifts) peaks of $s \rightarrow p$ PCS while it redshifts (blueshifts) those involving higher states. The ability of these potentials to modify transition energies without altering the sizes of SQDs avails nanotechnology immense control over tunability of these structures, through appropriate nano patterning.

I would like to express my sincere gratitude to G.A. Nkoni for editing of this paper.

References

1. N. Invernizzi, G. Foladori, E. Robles-Belmont, E.L. Záyago, E.A. Figueroa, C. Baagattolli, T.J. Carrozza, A. Chiancone, W. Urquijo, J. Nanopart. Res. **17**, 233 (2015)
2. G. Chandrasekaran, A. Sundararaj, H.A. Therese, K. Jeganathan, J. Nanopart. Res. **17**, 233 (2015)
3. G. Kang, J. Yoo, J. Ahn, K. Kim, Nano Today **10**, 22 (2015)
4. A.K. Rishinaramangalam, S.M. Ul Masabih, M.N. Fairchild, J.B. Wright, D.M. Shima, G. Balakrishnan, I. Brener, S.R.J. Brueck, D.F. Feezell, J. Electron Mater. **44**, 1255 (2015)
5. G. Pennelli, Eur. Phys. J. B **88**, 121 (2015)
6. S. Cecchi, L.F. Llin, T. Etzelstorfer, A. Samarelli, Eur. Phys. J. B **88**, 70 (2015)
7. L. Yang, W. Xie, Physica B **407**, 3884 (2012)
8. L.M. Burileanu, J. Lumin. **145**, 684 (2014)
9. W. Xie, Superlattices Microstruct. **63**, 10 (2013)
10. W. Xie, Superlattices Microstruct. **65**, 271 (2014)
11. C.T. Jin M, Xie W, Superlattices Microstruct. **62**, 59 (2013)
12. M.G. Barseghyan, A. Hakimyfard, M. Zuhair, C.A. Duque, A.A. Kirakosyan, Physica E **44**, 419 (2011)
13. W. Xie, Phys. Lett. A **377**, 903 (2013)
14. E.C. Niculescu, M. Cristea, J. Lumin. **135**, 120 (2013)
15. E.R. Arriola, J.S. Dehesa, J. Comput. Appl. Math. **37**, 169 (1991)
16. E.S. Cheb-Terrab, J. Phys. A **37**, 9923 (2004)